CrossMark

Self-coupled dual-mode ring resonator with turning transmission zeros in microwave bandpass filter for planar metamaterial: analysis and design

Ching-Chien Cheng[1] · Kong-Xin Cheng[1] · Huang-Kuang Kung[1] ·
Chin-Yu Wang[1] · Yng-Huey Jeng[2] · Sheng-Lung Tu[3] ·
Chun-Chieh Huang[4]

Abstract An H-shape dual-mode closed resonator with self-coupled segments is reported. The self-coupling between ring segments renders an equivalent mode perturbation effect as the normal ways of adding stub, cutting notch, or varying line impedance to the ring resonator. The mode perturbation and transmission-zero generation from the self-coupling effect and step-impedance were analyzed using the even–odd mode theory. By regulating the impedance ratio and coupling coefficients of self-coupled sections, the self-coupled ring resonator can produce either the capacitive or inductive perturbation. The input and output positions affect the number and locations of transmission zero. The positions of input and output ports are properly selected. In the capacitive perturbation case, when the two transmission zeros are located on both sides of the passband, and bring about a pseudo-elliptic bandpass response. The analysis of finding optimized taping positions of input and output ports is proposed. Comparing to the regular uniform ring resonator, the H-shaped self-coupled ring resonator has shorter ring length, is easily to be folded and does not destroy the dual-mode characteristics. The feature of compact size is favorable in the design of a bandpass filter. A 2.45-GHz bandpass filter based on the H-shaped self-coupled ring resonator was performed to verify the proposed theory. A schematic bandpass filter was implemented with a compact size which is only 20% of the conventional dual-mode bandpass filter.

✉ Chun-Chieh Huang
    k0590@gcloud.csu.edu.tw

[1] Institute of Mechatronics Engineering, Cheng Shiu University, Kaohsiung City, Taiwan

[2] Department of Electronic Engineering, National Formosa University, Yunlin, Taiwan

[3] Department of Resources Engineering, National Cheng Kung University, Tainan, Taiwan

[4] Department of Electrical Engineering, Cheng Shiu University, Kaohsiung, Taiwan

⚛ Springer

1 Introduction

Researches on microwave bandpass filter have been reported in many papers (Wolff and Knoppik 1971; Wolff 1972; Matsuo et al. 2001; Gorur 2002; Gorur et al. 2003; Tan et al. 2005; Miguel et al. 2012; Feng et al. 2015; Gorur 2004; Lin et al. 2012; Athukorala and Budimir 2009; Jeng et al. 2006; Takan et al. 2015; Demirhan et al. 2016), and the related materials also published (Cameron 2003; Amari and Rosenberg 2001; Amari 2004; Hsieh and Chang 2002, 2003; Hong and Lancaster 1996; Chen et al. 2017; Chen and Jiang 2016; Chen and Yang 2016). The bandpass filters based on the dual-mode ring resonator have been extensively investigated since the first analysis of dual-mode characteristic of the ring resonator by Wolff and Knoppik (1971). The uniform ring resonator has a degenerate mode, which is orthogonal and produces identical resonant frequencies. When this uniform ring resonator is input with an asymmetric arrangement of feeding lines with the circuit profile perturbed and the degenerate mode becomes coupled, a narrow-band bandpass response occurs (Wolff 1972). Based on this mode perturbation mechanism, numerous dual-mode bandpass filters have been reported. The different perturbation schemes include (a) the distributed perturbation which uses step-impedance ring resonator (Matsuo et al. 2001; Lin et al. 2012); (b) the capacitive perturbation which leads to elliptic response, by the addition of single or multiple open stubs symmetrically on the ring (Gorur 2002; Gorur et al. 2003; Tan et al. 2005; Feng et al. 2015); (c) the inductive perturbation by cutting single or multiple notches on the ring (Wolff 1972; Tan et al. 2005; Gorur 2004; Lin et al. 2012; Athukorala and Budimir 2009).

In a previous study, Jeng et al. (2006) proposed a distributed perturbation scheme by coupling adjacent segments of the ring resonator. This scheme has the advantage of easy implementation, since extra stubs or notches are not needed. Furthermore, the self-coupled ring resonator can shift the resonant frequency toward the lower frequencies such that the circuit size can be reduced. In this study we propose an H-shaped dual-mode closed resonator with the distributed perturbation scheme. It has the same benefit of taking shorter ring length and can be easily folded but does not destroy the dual-mode characteristic. In Sect. 2, the mode perturbation owning to the self-coupled effect is analyzed. In Sect. 3, the generation and number of transmission zero are discussed. Since the periphery was not a simple round ring, to have transmission zeros symmetric to the passband, the optimum angle between input and output ports will not be 90 degrees anymore. The method of finding optimized taping positions of input and output ports is proposed. Bandpass filter applications with the proposed H-shaped self-coupled ring resonator and its folded schematic were described in Sect. 4, where the simulation and measurement results are discussed in detail and the transmission zeros by simulation and measurement is compared to the calculation one. Finally, a conclusion is given in Sect. 5.

2 Mode perturbation

The schematic diagram of the proposed self-coupled ring resonator is composed of a coupled pair at the center section and two coupled pairs at the two ends shown in Fig. 1a. The central coupled section has a physical length of $2\ell_2$, a coupling coefficient of c_2, and a
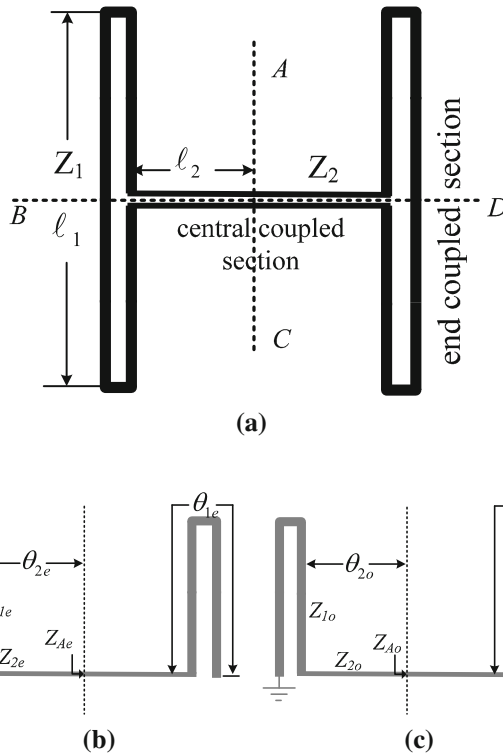
Fig. 1 Proposed self-coupled ring resonator, **a** schematic, **b** even-mode equivalent circuit, **c** odd-mode equivalent circuit

characteristic impedance of Z_2. The two end coupled sections have the same parameters: physical lengths of ℓ_1, coupling coefficients of c_1, characteristic impedances of Z_1. The structure is symmetric to line $\overline{BD}$ and line $\overline{AC}$. In the following derivation, the effect of layout discontinuity is neglected.

2.1 Resonance conditions

Because the structure is symmetric with respect to line $\overline{BD}$, the resonance condition can be derived using the even–odd mode theory with $\overline{BD}$ as the reference plane. Following the processes of Jeng et al. (2006), the equivalent even- and odd-mode circuits obtained from the replacement of the reference plane $\overline{BD}$ with the magnetic and electric walls are respectively given in Fig. 1b, c. Let the impedance ratio $R = Z_1/Z_2$ be the ratio of the characteristic impedances of the end coupled section to the central coupled section. Then the even-mode and odd-mode resonance conditions can be expressed as:

$$\tan\theta_{1e}\tan\theta_{2e} = R\sqrt{\frac{1-c_2}{1+c_2}} \cdot \frac{1+c_1\sec\theta_{1e}}{\sqrt{1-c_1^2}}, \tag{1}$$

$$\tan \theta_{1o} \tan \theta_{2o} = \frac{1}{R} \sqrt{\frac{1 - c_2}{1 + c_2}} \cdot \frac{1 + c_1 \sec \theta_{1o}}{\sqrt{1 - c_1^2}}, \tag{2}$$

where θ_{1e}, θ_{2e}, θ_{1o} and θ_{2o} are the electrical lengths corresponding to the physical lengths ℓ_1 and ℓ_2 at the even-mode resonant frequency f_{re} and the odd-mode resonant frequency f_{ro}, respectively. The even-mode and odd-mode impedances of parallel-coupled lines were used in the relationship of the coupling coefficient and characteristic impedance:

$$c_1 = \frac{Z_{1e} - Z_{1o}}{Z_{1e} + Z_{1o}}, \ Z_1 = \sqrt{Z_{1e}Z_{1o}}, \text{ and } c_1 = \frac{Z_{1e} - Z_{1o}}{Z_{1e} + Z_{1o}}, \ Z_2 = \sqrt{Z_{2e}Z_{2o}}.$$

From the derived resonance conditions (1) and (2), it is revealed that the even and odd modes are splitted because of the impedance change and the self-coupling of the ring. The impedance ratio R and the coupling coefficients, c_1 and c_2, determine the nature (capacitive or inductive) of the extent splitting mode.

2.2 Effect of impedance ratio R

By solving Eqs. (1) and (2), the even-mode and odd-mode resonant frequencies with the impedance ratio and coupling coefficients can be obtained. The dependence of mode resonant frequencies on impedance ratio is shown in Fig. 2 by an exemplary case of $c_1 = 0.2$ and $c_2 = 0.4$. For the situation of capacitive perturbation ($R < 1$), the odd-mode resonant frequency is higher than the even-mode. On the contrary, for the inductive perturbation situation ($R > 1$), the odd-mode frequency is lower than the even mode. The variation of even-mode and odd-mode resonant frequencies increases when impedance ratio R deviates further from 1. However, the geometric mean of resonant frequencies, $f_{r,SCR} = \sqrt{f_{re}f_{ro}}$, is unaffected by the impedance ratio.

2.3 Effect of coupling coefficient

To examine the effect of self coupling through the central section and end sections, the resonance conditions (1) and (2) are solved for six different situations and drawn in Fig. 3.

Fig. 2 Normalized resonant frequencies with respect to the impedance ratio R
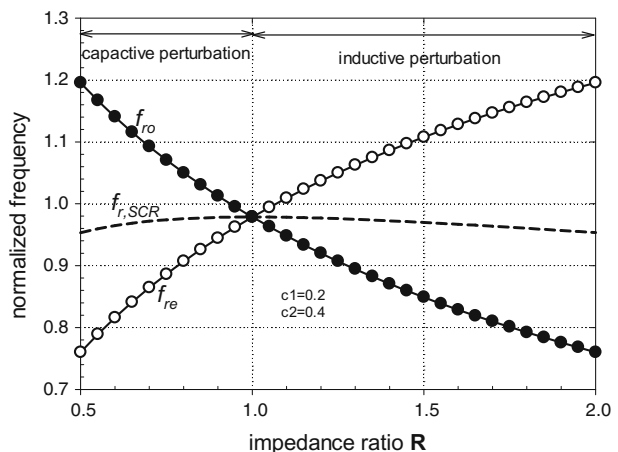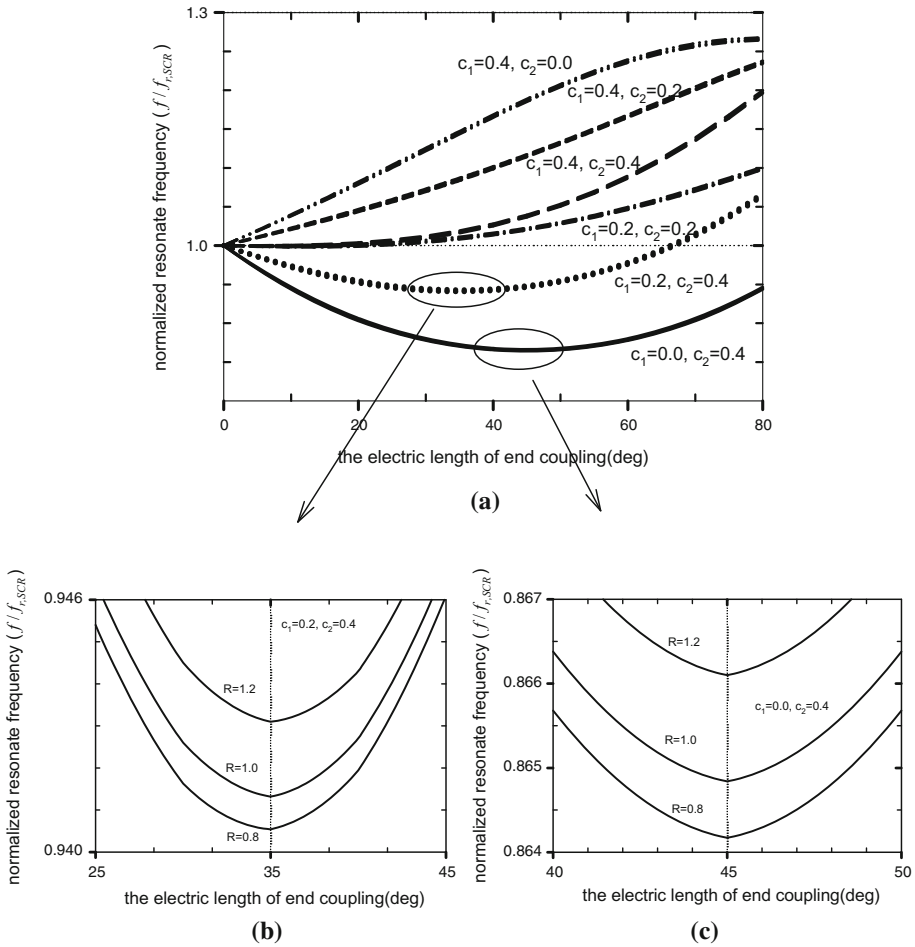
Fig. 3 Calculated normalized resonant frequencies with respect to the electric length θ_1 **a** wider range, **b** small scope for cases of $c_1 = 0.2$, $c_2 = 0.4$, **c** small scope for cases of $c_1 = 0$, $c_2 = 0.4$

In Fig. 3, the lines for $R = 0.8$, $R = 1.0$ and $R = 1.2$ are almost coincide, indicating the geometric average resonant frequency, $f_{r,SCR} = \sqrt{f_{re}f_{ro}}$, is insensitive to the impedance ratio R but susceptible to the coupling coefficient c_1 and c_2. Figure 3a shows that, the average resonant frequency $f_{r,SCR} = \sqrt{f_{re}f_{ro}}$ decrease in both capacitive and inductive perturbations with the increasing of the central self-coupling coefficient c_2 and the decreasing of the end self-coupling coefficient c_1. Based on the ring resonator with a dominant central self-coupling, a bandpass filter has a smaller circuit size than the filters with uncoupled uniform ring resonator. Furthermore, for the case of $c_2 > c_1$, there exists a $\theta_{1,min}$ with a minimum geometric average resonant frequency, $f_{r,SCR} = \sqrt{f_{re}f_{ro}}$, and for the case of $c_2 \leq c_1$, $\theta_{1,min}$ approaches zero for either capacitive or inductive perturbations. In the case c_1, shown in Fig. 3c, the minimum geometric average resonant frequency occurs at $\theta_{1,min} = 45°$, which is similar to the structure proposed in the report of Jeng et al. (2006), but for the case of $c_2 = 0.2$, $c_2 = 0.4$, shown in Fig. 3b, the minimum geometric average resonant frequency occurs at $\theta_{1,min} = 35°$. Therefore, the value of $\theta_{1,min}$ is a function of c_1

and c_2, but almost independence of impedance ratio R, and the ring resonator based on the dominant central self-coupling has the smallest resonate frequency.

3 Transmission zeros

We name the electric length between input and output ports as θ_{IO}. Unlike the conventional ring bandpass filter, the optimized angle θ_{IO} of the H-type bandpass filter, with the transmission zeros symmetric to the passband, is not 90° any more. We can turn locations of transmission-zeros by the parameter θ_{IO}, end coupling length, θ_1 and impedance ratio, R. To examine how θ_{IO}, θ_1 and R affect the existence and distribution of transmission-zeros, the coupling matrix method (Hong and Lancaster 2001; Cameron 2003; Amari and Rosenberg 2001) and the admittance matrix method (Matsuo et al. 2001; Gorur 2004) have been used. The following result is that the admittance matrix method is adopted.

First, consider the case of $\theta_{IO} < \theta_1$: Referred to Fig. 4a, the trans-admittance of the self-coupled ring resonator can be obtained as below:

$$Y_{21} = Q_L + Q_{ac} \frac{U(G_L + P_R) - W(H_L + Q_R)}{(H_L + Q_R)^2 - (G_L + P_R)^2}, \tag{3}$$

where

$$P_R = P_2 - \frac{2P_1 P_2^2 [2c_2^2 (2P_1 Q_2 - Q_1^2) + (1 + c_2^2)(2P_1^2 - Q_1^2 + 2P_1 P_2)]}{\cos^2 2\theta_2 [(2P_1^2 - Q_1^2 + 2P_1 P_2)^2 - (2P_1 Q_2 - Q_1^2)^2]},$$

$$Q_R = Q_2 + \frac{2P_1 P_2^2 [2c_2^2 (2P_1^2 - Q_1^2 + 2P_1 P_2) + (1 + c_2^2)(2P_1 Q_2 - Q_1^2)]}{\cos^2 2\theta_2 [(2P_1^2 - Q_1^2 + 2P_1 P_2)^2 - (2P_1 Q_2 - Q_1^2)^2]},$$

$$P_1 = -\frac{jY_1 \cot \theta_1}{\sqrt{1 - c_1^2}}(1 + c_1 \sec \theta_1), \quad Q_1 = \frac{jY_1 \cot \theta_1}{\sqrt{1 - c_1^2}}(c_1 + \sec \theta_1),$$

$$P_2 = -\frac{jY_2}{\sqrt{1 - c_2^2}}\cot 2\theta_2, \quad Q_1 = \frac{jY_1 c_2}{\sqrt{1 - c_2^2}}\cot 2\theta_2.$$
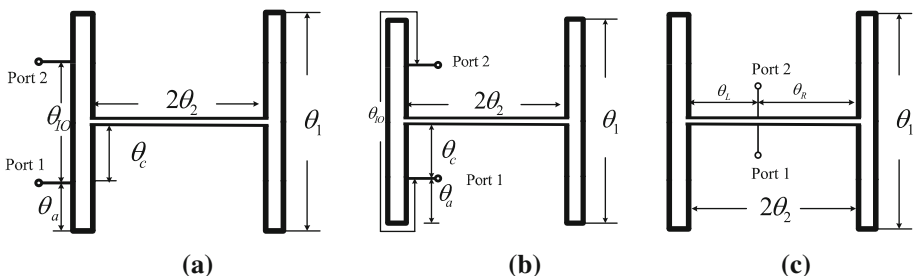

Fig. 4 Self-coupled ring resonator for **a** $\theta_{IO} < \theta_1$, **b** $\theta_1 < \theta_{IO} < 2\theta_1$ and **c** $2\theta_1 < \theta_{IO} < \frac{\pi}{2}$

$$Q_L = Q_{ac} \frac{(1 - c_1^2) \sin^2(2\theta_a + \theta_c)}{2M \sin \theta_c}, \quad G_L = -\frac{Q_{ac}}{\sin \theta_c} \frac{J(2M - c_1^2 J)}{2(1 - c_1^2)M},$$

$$H_L = \frac{Q_{ac}}{\sin \theta_c} \frac{c_1^2 J}{2(1 - c_1^2)M},$$

$$Q_{ac} = \frac{jY_1 \sqrt{(1 - c_1^2)}}{[c_1 \sin \theta_c + \sin(2\theta_a + \theta_c)]},$$

$$U = \frac{c_1 J \sin(2\theta_a + \theta_c)}{2(M \sin \theta_c)^2} [2M \sin \theta_c + c_1 J \sin(2\theta_a + \theta_c)]$$

$$W = \left[\frac{c_1 J \sin(2\theta_a + \theta_c)}{2M \sin \theta_c}\right]^2 + [2M \sin \theta_c + c_1 J \sin(2\theta_a + \theta_c)]^2$$

$$J = [c_1 \sin \theta_c + \sin(2\theta_a + \theta_c)] \cos \theta_c - \sin 2\theta_a,$$
$$M = [c_1 \sin \theta_c + \sin(2\theta_a + \theta_c)] \cos \theta_c - c_1^2 \sin 2\theta_a,$$

Second, consider the case of $\theta_1 < \theta_{IO} < 2\theta_1$: Referred to Fig. 4b, the self-coupled ring resonator has the same trans-admittance equation as (3) but different parameters as below:

$$U = c_1 \left[c_1 + \frac{2 \sin(2\theta_a + \theta_c)}{\sin \theta_c}\right],$$

$$W = \frac{c_1^2}{4} + \left[\frac{\sin(2\theta_a + \theta_c)}{\sin \theta_c} + \frac{c_1}{2}\right],$$

$$Q_L = Q_{ac} \frac{\sin \theta_c}{2J} (1 - c_1^2), \quad G_L = \frac{Q_{ac}}{\sin \theta_c} \left[\frac{J(c_1^2 - 2)}{2(1 - c_1^2)} - \sin 2\theta_a\right], \quad H_L = \frac{Q_{ac}}{\sin \theta_c} \frac{c_1^2 J}{2(1 - c_1^2)},$$

Third, consider the case of $2\theta_1 < \theta_{IO} < \frac{\pi}{2}$: Referred to Fig. 4c and following the driving process in Jeng et al. (2006), the trans-admittance of the self-coupled ring resonator can be obtained as:

$$Y_{21} = Y_{21} + Y_{21R}, \tag{4}$$

where

$$Y_{21R} = Q_R + 2P_1 \frac{(S_R^2 + T_R^2)(2P_1 Q_R - Q_1^2) - 2S_R T_R(2P_1^2 - Q_1^2 + 2P_1 P_R)}{(2P_1^2 - Q_1^2 + 2P_1 P_R)^2 - (2P_1 Q_R - Q_1^2)^2}$$

$$Y_{21L} = Q_L + 2P_1 \frac{(S_L^2 + T_L^2)(2P_1 Q_L - Q_1^2) - 2S_L T_L(2P_1^2 - Q_1^2 + 2P_1 P_L)}{(2P_1^2 - Q_1^2 + 2P_1 P_L)^2 - (2P_1 Q_L - Q_1^2)^2}$$

$$P_R = Y_2 \frac{-j}{\sqrt{1 - c_2^2}} \cot 2\theta_R \quad P_L = Y_2 \frac{-j}{\sqrt{1 - c_2^2}} \cot 2\theta_L$$

$$Q_R = Y_2 \frac{jc_2}{\sqrt{1 - c_2^2}} \cot 2\theta_R \quad Q_L = Y_2 \frac{jc_2}{\sqrt{1 - c_2^2}} \cot 2\theta_L$$

$$S_R = Y_2 \frac{j}{\sqrt{1-c_2^2}} \csc 2\theta_R \quad S_L = Y_2 \frac{j}{\sqrt{1-c_2^2}} \csc 2\theta_L$$

$$T_R = Y_2 \frac{-jc_2}{\sqrt{1-c_2^2}} \csc 2\theta_R \quad T_L = Y_2 \frac{-jc_2}{\sqrt{1-c_2^2}} \csc 2\theta_L$$

The transmission zero exists if Y_{21} of (3) or (4) vanishes. (3) and (4) are too complex to get familiar form solution, the spectral response of Y_{21} for the cases of various impedance ratio R or θ_{IO} values with $c_1 = 0.2$ and $c_2 = 0.4$ is plotted from Figs. 5, 6, 7, 8, where the frequency axis is normalized with respect to the geometric average resonant frequency, $f_{r,SCR} = \sqrt{f_{re}f_{ro}}$.

3.1 Effect of the angle between input and output ports θ_{IO}

Figure 5 reveals that for a set of parameters, θ_1, R, c_1 and c_2, there exists a critical angle $\theta_{IO,\max}$ that when the angle θ_{IO} is smaller than $\theta_{IO,\max}$, there are two transmission zeros near the fundamental passband located at either side of the passband. Furthermore, both transmission zeros shift to high frequency as the angle θ_{IO} increased. When the angle θ_{IO} becomes greater than $\theta_{IO,\max}$, the transmission zero at the upper stopband disappears but the transmission zero at the lower stopband remains. Figure 5a, b were drawn with the same parameters R, c_1 and c_2, except $\theta_1 = 60°$ in Fig. 5a and $\theta_1 = 30°$ in Fig. 5b, where they have the similar tendency but $\theta_{IO,\max}$ dropped off from 124° to 114° as θ_1 decreased from 60° to 30°.

In order to make the transmission zeros distribution symmetric to the fundamental passband, the optimum angle $\theta_{IO,op}$ is 90° for traditional dual-mode ring resonator, but now its range is 100°–110° for H-type dual-mode ring resonator from Fig. 5.

3.2 Effect of impedance ratio R

Figure 6 is the spectral response of Y_{21} with $c_1 = 0.2$, $c_2 = 0.4$, $\theta_1 = 30°$, and θ_{IO} varying form 90° to 110°, when $\theta_{IO} = 110°$ and when $R = 1$ there exists only one transmission
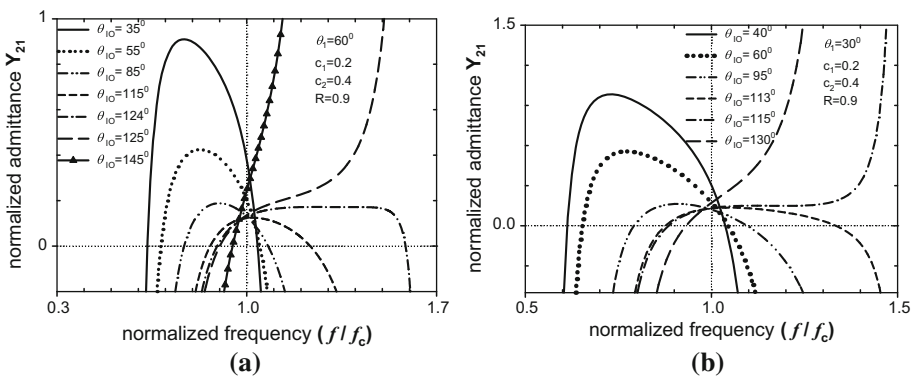

Fig. 5 Spectral response of Y_{21} of the self-coupled ring resonator versus the various value of θ_{IO} in the case of $c_1 = 0.2$, $c_2 = 0.4$, $R = 0.9$ and **a** $\theta_1 = 60°$, **b** $\theta_1 = 30°$

Fig. 6 Spectral response of Y_{21} of the self-coupled ring resonator versus the various value of θ_{IO} in the case of $c_1 = 0.2$, $c_2 = 0.4$, and $\theta_1 = 30°$
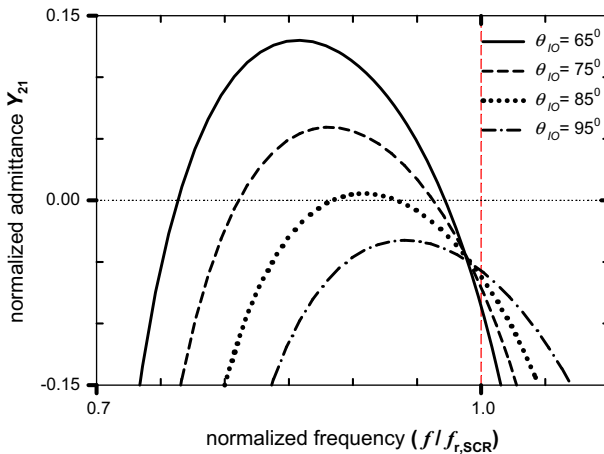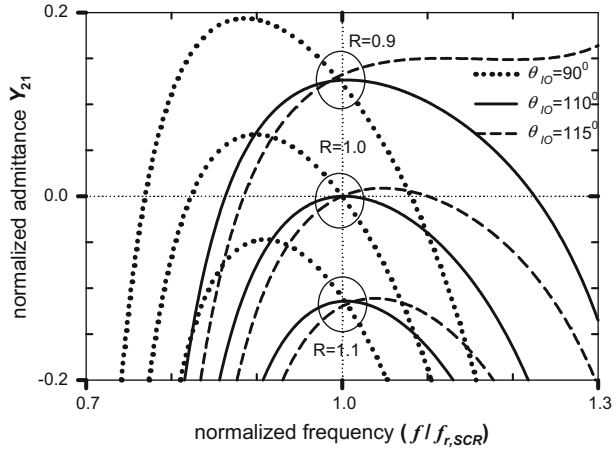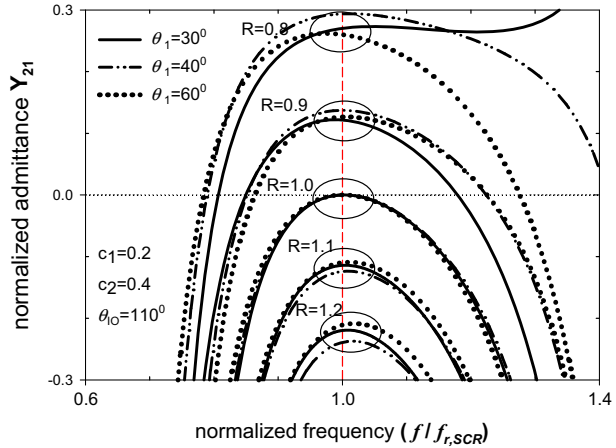

Fig. 7 Spectral response of Y_{21} of the self-coupled ring resonator versus the various value of θ_{IO} in the case of $c_1 = 0.2$, $c_2 = 0.4$, $R = 1.05$, and $\theta_1 = 60°$

zero coinciding with the geometric average resonant frequency, $f_{r,SCR}$, which destroys the resonating condition. When R decreases from one, it enters the capacitive perturbation situation, and two transmission zeros near the fundamental passband are created, each located at either side of the passband. If R increases from one, it becomes the inductive perturbation situation, and both two transmission zeros disappear. This observation is similar with the result found in Jeng et al. (2006), Amari and Rosenberg 2001). But when θ_{IO} departs from $\theta_{IO,op}$, for the case of R < 1, those two transmission zeros remain. When $R = 1$, there still exists two transmission zeros, with one of which coinciding with the geometric average resonant frequency, $f_{r,SCR}$, resulting in destroyed inband performance. Even if $R > 1$, there is still the opportunity to get two transmission zeros in the same stopband, and it can be applied to suppress undesired wideband signal. Fig 7 presents the spectral response of Y_{21} of the self-coupled ring resonator *vs.* the variation of θ_{IO} value for

Fig. 8 Spectral response of Y_{21} of the self-coupled ring resonator versus the various value of θ_1 in the case of $c_1 = 0.2$, $c_2 = 0.4$, and $\theta_{IO} = 110°$

$c_1 = 0.2$, $c_2 = 0.4$, $R = 1.05$, and $\theta_1 = 60°$. While for $\theta_{IO} \leq 85°$, there exists two transmission zeros in the lower stopband.

3.3 Effect of the electric length of end coupling θ_1

Figure 8 shows the spectral response of Y_{21} with respect to the various value of R and θ_1 in the case of $c_1 = 0.2$, $c_2 = 0.4$, and $\theta_{IO} = 110°$ and there is only one transmission zero for case of $R = 1$, that is, $\theta_{IO,op}$ is insensitive to the length of end coupling θ_1. In practical application, the range R will be 0.9–1.1, and $\theta_{IO,op}$ could adopt about $100°–110°$ in H-shape resonator design.

To examine the effect of the electric length of end sections upon the location of transmission zeros, the spectral response of Y_{21} was drawn in Fig. 9 with the various value of θ_1 in the case of $c_1 = 0.2$, $c_2 = 0.4$, $R = 0.9$ and $\theta_{IO} = 110°$. In Fig. 9a, the input and output ports are located in the central section, and from Fig. 3b, the angle $\theta_{1,min}$ with a minimum geometric average resonant frequency, $f_{r,SCR} = \sqrt{f_{re}f_{ro}}$, equals to $35°$. When θ_1 increases and $\theta_1 < \theta_{1,min}$, the transmission zeros go away from $f_{r,SCR}$, contrarily, as θ_1
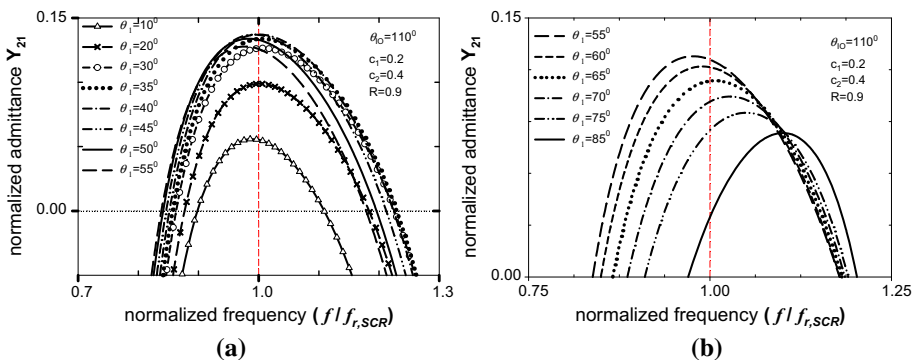

Fig. 9 Spectral response of Y_{21} of the self-coupled ring resonator versus the various value of θ_1 in the case of $c_1 = 0.2$, $c_2 = 0.4$, $R = 0.9$, and $\theta_{IO} = 110°$ for **a** the input and output ports are located in the central section, **b** the input and output ports are located in the end sections

increases and $\theta_1 > \theta_{1,min}$, the upper transmission zero changes direction to approach $f_{r,SCR}$, but the location of the lower transmission zero almost remains. In Fig. 9b, the input and output ports are located in the end sections, when θ_1 increases, both the transmission zeros go to high frequencies, and the lower transmission zero shifts more quickly than the upper transmission zero. Furthermore, when θ_1 approaches 90°, the response, Y_{21}, becomes more unsymmetrical.

4 Bandpass filter application

A 2.45-GHz bandpass filter was designed with a proposed self-coupled ring resonator on a Rogers 25 N substrate. The substrate has a dielectric constant ε_r of 3.38, loss tangent of 0.0025, and a dielectric layer thickness of 762 µm, and then the circuit was implement. The design procedures are described from Sects. 4.1–4.3.

4.1 Initial dimension estimation

From the result in Sect. 3, to produce pseudo-elliptic filter performance, the capacitive perturbation was selected. An impedance ratio of $R = 0.9$ was chosen. To minimize the ring size and consider constrains, in practice the ring structure with dominant central self-coupling, $c_2 = 0.395$ and $c_1 = 0.197$ was chosen. The even- and odd-mode normalized resonant frequencies are 0.97 and 1.03. Substituting these two values into Eqs. (1) and (2) and for the purpose of folding the end sections easily, we put $\theta_1 = 66°$ and $\theta_1 = 24°$ at normalized frequency, then the geometric average resonant frequency, $f_{r,SCR}$ will be equal to 0.998. Therefore, we obtain the initial circuit dimensions by transforming $f_{r,SCR}$ to 2.45 GHz and designing the H-type and folding EC-type bandpass filters with the same resonator structure. The input and output tapping positions are obtainted by solving $Y_{21} = 0$ to get $\theta_{IO} = 113°$, as discussed in Sect. 3. The calculated transmission zeros are 2.078, 2.782 and 5.505 GHz. The circuit layout and electromagnetic simulation are discussed in the following sections.
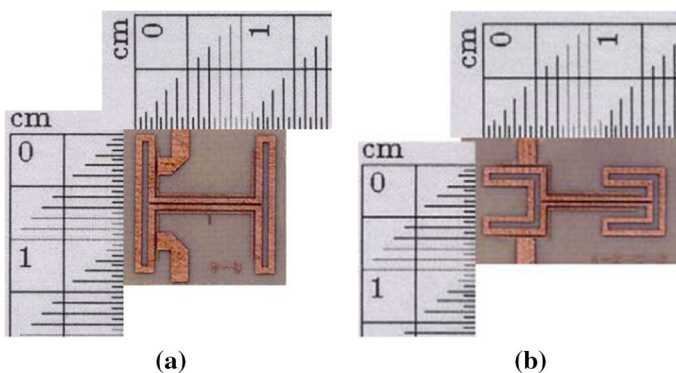

(a)   **(b)**

Fig. 10 Photos of 2.45-GHz dual-mode bandpass filter **a** H-shape, **b** foldes EC-shape

4.2 Layout

The layout scheme is illustrated in Fig. 10. The filter dimensions are 13.6×14.2 mm^2 and 7×17.4 mm^2 for H-shape and folded type, which are 35 and 20% of the dimension of the conventional dual-mode bandpass filter, respectively.

4.2.1 3D electromagnetic simulation

The electromagnetic simulator IE3D was designed to include dielectric loss, conductor loss, spurious coupling, and finite ground plane effects. The simulation results are shown by the dash lines in Figs. 11 and 12, where the simulation insertion loss is less than 0.8, 0.78 dB and the return loss is better than 17.5, 19 dB for H-type and folded type, respectively, in the range 2.4–2.5 GHz. The transmission zeroes locate at 2.085, 2.89, 4.105, 5.075 GHz and 2.12, 2.855, 4.945, 5.375 GHz, on both side of passband. The simulated results show that this filter belongs to a second-order filter. If higher-order response is needed, a cross-coupled arrangement as reported in Hsieh and Chang (2003), Hsieh and Chang (2002), Hong and Lancaster (1996) with such resonator can be used.

4.3 Measurement

The SMA connector connected to the vector network analyzer to obtain the scattering parameters is used for the measurement. The measured results are illustrated by the solid line in Figs. 11 and 12, in which the measured insertion loss is less than 1.4, 1.15 dB and the return loss is better than 10.5, 13.5 dB, in the range of 2.4 GHz from to 2.5 GHz for H-type and folded one, respectively. The measured passband range is 2.4–2.5 GHz, which dovetails with the simulation result.

The transmission zeros are located at 2.059, 2.852, 4.092, 5.035 and 2.108, 2.828, 4.886, 5.332 GHz, on both side of passband for H-type and folded one, respectively. The measured transmission zeros, i.e. 2.059, 2.852, 5.035 and 2.108, 2.828, 5.332 GHz corresponding to 2.085, 2.89, 5.075 and 2.12, 2.855, 5.375 GHz of simulated results for H-type and folded type respectively closely match the resonator inherent transmission zeros 2.078, 2.782 and 5.505 GHz calculated by Eq. (3) with the same input and output ports positions.

Fig. 11 Measurement and simulation results of the H-shape bandpass filter using the self-coupled ring resonator with $R = 0.9$, $\theta_1 = 66°$, $\theta_2 = 24°$, $c_1 = 0.197$ and $c_2 = 0.395$
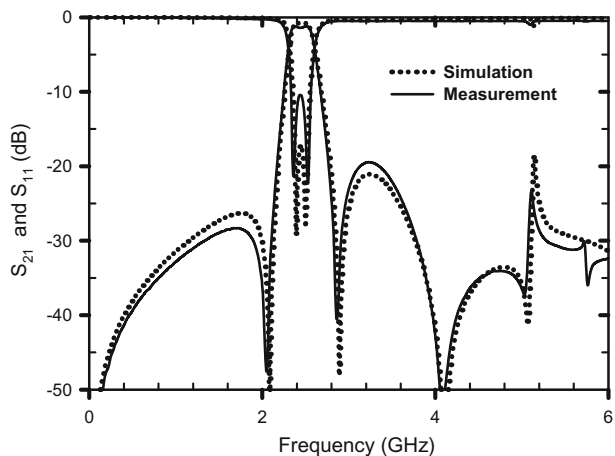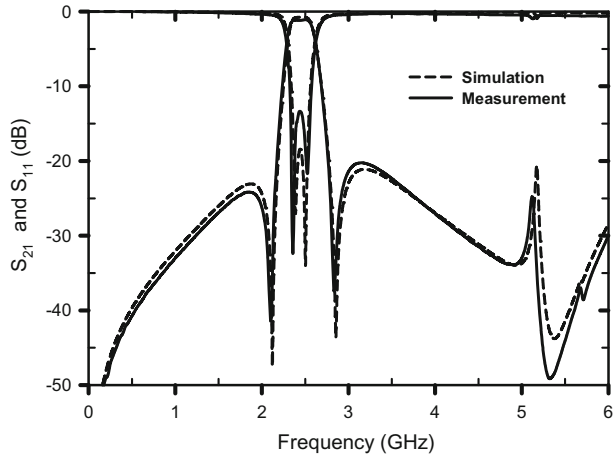
Fig. 12 Measurement and simulation results of the EC-shape bandpass filter using the self-coupled ring resonator with $R = 0.9$, $\theta_1 = 66°$, $\theta_2 = 24°$, $c_1 = 0.197$ and $c_2 = 0.395$

The stopband performance comparisons of the measurement and simulation to the calculated results of transmission zeros are listed in Tables 1, 2 for H-shape and folded EC-shape bandpass filters. The shift is defined as: $shifting = \frac{(f_{zn,res} - f_{zn,cal})}{f_{zn,cal}} \times 100\%$, where $f_{zn,res}$ is the nth transmission zero frequency of simulated or measured results and $f_{zn,cal}$ is the nth transmission zero frequency calculated by Eq. (3). We can find that the shift of transmission zero frequencies near passband are all less than 4% and the shift of the 4th transmission zero frequencies are still within 9%. It can be concluded that the 1st, 2nd and 4th transmission zeros are from the resonator structure and Eqs. (3) and (4) are useful for a dual mode bandpass filters design.

Table 1 Transmission zeros compare of the measurement and simulation to calculated results for H-shape (GHz)

No.	Calculation	Simulation	Shift	Measurement	Shift
f_{z1}	2.078	2.085	+0.33%	2.059	−0.93%
f_{z2}	2.780	2.890	+3.86%	2.852	+2.51%
f_{z3}	–	4.105	–	4.092	–
f_{z4}	5.574	5.07	−7.90%	5.035	−8.54%

Table 2 Transmission zeros compare of the measurement and simulation to calculated results for folded EC-shape (GHz)

No.	Calculation	Simulation	Shift	Measurement	Shift
f_{z1}	2.078	2.120	+2.01%	2.108	+1.45%
f_{z2}	2.780	2.890	+2.60%	2.828	+1.62%
f_{z3}	–	4.945	–	4.886	–
f_{z4}	5.574	5.375	−2.36%	5.332	−3.14%

5 Conclusions

A new dual-mode ring resonator, which is composed of one central coupled section connected to two identical coupled sections at both ends, is proposed. The central coupled section has a coupling coefficient c_2, a characteristic impedance Z_2, and a length $2\ell_2$. The coupled sections at both ends have the same coupling coefficient c_1, the characteristic impedance Z_1 and the length ℓ_1. The mode splitting mechanism is derived from the change of the ring characteristic impedance and the self-coupling through the central and end sections. The perturbation nature is fundamentally determined by the impedance ratio R. The capacitive perturbation is generated by $R < 1$ and the inductive perturbation by $R > 1$. The larger the impedance ratio, the greater the frequency difference between the even and odd modes. The average resonant frequency of the even- and odd-mode is insensitive to the impedance ratio. However, it decreases with the central coupling coefficient c_2 and increases with the end coupling coefficient c_1.

According to specifications requirement, the transmission zeros, on both or the same side of passband, are proved to exist only for proper combination of R, c_1, c_2 and θ_1. This article proposed an analysis method to save the trial-and-error time.

Two bandpass filters were designed with the proposed self-coupled ring resonator of $R = 0.9$, $c_1 = 0.197$ and $c_2 = 0.395$. The circuit sizes are only 35 and 25% of the uncoupled uniform ring case. The measured insertion loss is less than 1.4, 1.15 dB and the return loss is better than 10.5, 13.5 dB for H-type and folded EC shape one, respectively, in the range 2.4–2.5 GHz, which dovetails with the simulation result. The measurement transmission zeros 2.059, 2.852, 5.035 GHz for H-type and 2.108, 2.828, 5.332 GHz for folded type corresponded to 2.085, 2.89, 5.075 and 2.12, 2.855, 5.375 GHz of simulated results respectively, closely matching the resonator inherent transmission zeros 2.078, 2.782 and 5.505 GHz calculated by our proposed formulas with the same input and output ports positions. The shift of transmission zero frequencies near passband is less than 4% and the shift of the 4th transmission zero frequencies is still within 9%, and we can conclude the 1st, 2nd and 4th transmission zeros come from the resonator structure. The implement results show the analysis method can be used to design the bandpass filter and forecast its implement precisely.

References

Amari, S.: Comments on description of coupling between degenerate modes of a dual-mode microstrip loop resonator using a novel perturbation arrangement and its dual-mode bandpass filter applications. IEEE Trans. Microwav. Theor. Tech. **52**, 2190–2192 (2004)

Amari, S., Rosenberg, U.: Direct synthesis of a new class of bandstop filters with source-load coupling. IEEE Microwav. Wirel. Compon. Lett. **11**, 264–266 (2001)

Athukorala, L., Budimir, D.: Compact dual-mode open loop microstrip resonators and filters. IEEE Microw. Wirel. Compon. Lett. **19**, 698–700 (2009)

Cameron, R.J.: Advanced coupling matrix synthesis techniques for microwave filters. IEEE Trans. Microwav. Theor. Tech. **51**, 1–10 (2003)

Chen, T.H., Jiang, B.L.: Optical and electronic properties of Mo:ZnO thin films deposited using RF magnetron sputtering with different process parameters. Opt. Quant. Electron. **48**(2), 77 (2016). doi:10. 1007/s11082-015-0357-1

Chen, T.H., Yang, C.L.: The Mg doping GZO thin films for optical and electrical application by using RF magnetron sputtering. Opt. Quant. Electron. **48**(12), 533 (2016). doi:10.1007/s11082-016-0808-3

Chen, T.H., Jiang, B.L., Huang, C.T.: The optical and electrical properties of MZO transparent conductive thin films on flexible substrate. Smart Sci. **5**, 53–60 (2017)

Demirhan, Y., Alaboz, H., Ozyuzer, L., Nebioglu, M.A., Takan, T., Altan, H., Sabah, C.: Metal mesh filters based on Ti, ITO and Cu thin films for terahertz waves. Opt. Quant. Electron. **48**(2), 170 (2016). doi:10.1007/s11082-016-0427-z

Feng, W., Gao, X., Che, W., Xue, Q.: Bandpass filter loaded with open stubs using dual-mode ring resonator. IEEE Microw. Wirel. Compon. Lett. **25**, 295–297 (2015)

Gorur, A.: A novel dual-mode bandpass filter with wide stopband using the properties of microstrip open-loop resonator. IEEE Microwav. Wirel. Compon. Lett. **12**, 386–388 (2002)

Gorur, A.: Description of coupling between degenerate modes of a dual-mode microstrip loop resonator using a novel perturbation arrangement and its dual-mode bandpass filter application. IEEE Trans. Microwav. Theor. Tech. **52**, 671–677 (2004)

Gorur, A., Karpuz, C., Akpinar, M.: A reduced-size dual-Mode bandpass filter with capacitively loaded open-loop arms. IEEE Microw. Wirel. Compon. Lett. **13**, 385–387 (2003)

Hong, J.S., Lancaster, M.J.: Compact microwave elliptic function filter using novel microstrip meander open-loop resonators. Electron. Lett. **32**, 563–564 (1996)

Hong, J.S., Lancaster, M.J.: Microstrip filter for RF/microwave applications. John Wiley & Sons, Inc., Hoboken, NY (2001)

Hsieh, L.-H., Chang, K.: Dual-mode quasi-elliptic-function bandpass filter using ring resonators with enhanced-coupling indeed tuning stubs. IEEE Trans. Microwav. Theor. Tech. **50**, 1340–1345 (2002)

Hsieh, L.-H., Chang, K.: Compact, low insertion-loss, sharp-rejection, and wide-band microstrip bandpass filters. IEEE Trans. Microwav. Theor. Tech. **51**, 1241–1246 (2003)

IE3D v10.1, Zeland Software, Inc., CA, USA

Jeng, Y.-H., Chang, S.-F., Chen, Y.-M., Huang, Y.-J.: A novel self-coupled dual-mode ring resonator and its applications to bandpass filters. IEEE Trans. Microwav. Theor. Tech. **54**, 2146–2152 (2006)

Lin, T.-W., Kuo, J.-T., Chung, S.-J.: Dual mode ring resonator bandpass filter with asymmetric inductive coupling and its miniaturation. IEEE Trans. Microwav. Theor. Tech. **60**, 2808–2814 (2012)

Matsuo, M., Yabuki, H., Makimoto, M.: Dual-mode stepped-impedance ring resonator for bandpass filter applications. IEEE Trans. Microwav. Theor. Tech. **49**, 1235–1240 (2001)

Miguel, D.S., Jordi, N., Ferran, P., Jordi, B., Ferran, M.: Electrically small resonators for planar metama-terial, microwave circuit and antenna design: a comparative analysis. Appl. Sci. **2**, 375–395 (2012)

Takan, T., Keskin, H., Altan, H.: Low-cost bandpass filter for terahertz applications. Opt. Quant. Electron. **47**(4), 953–960 (2015)

Tan, B.-T., Yu, J.-J., Chew, S.-T.: A miniaturized dual-mode ring bandpass filter with a new perturbation. IEEE Trans. Microwav. Theor. Tech. **53**, 343–348 (2005)

Wolff, I.: Microstrip bandpass filter using degenerate modes of a microstrip ring resonator. Electron. Lett. **8**, 302–303 (1972)

Wolff, I., Knoppik, N.: Microstrip ring resonator and dispersion measurements on microstrip lines. Electron. Lett. **7**, 779–781 (1971)